Heterogeneities along the 2009 L'Aquila normal fault inferred by the b-value distribution

Pasquale De Gori[1], Francesco Pio Lucente[1], Anna Maria Lombardi[2], Claudio Chiarabba[1] and Caterina Montuori[3]

Istituto Nazionale di Geofisica e Vulcanologia, Roma, Italy:

Centro Nazionale Terremoti [(1)];

Sezione di Roma 1 [(2)];

Sezione di Roma 2 [(3)]

Abstract

In this study we map the distribution of the b-value of the Gutenberg-Richter law—as well as complementary seismicity parameters—along the fault responsible for the 2009 M_W 6.1 L'Aquila earthquake. We perform the calculations for two independent aftershock sub-catalogs, before and after a stable magnitude of completeness is reached. We find a substantial spatial variability of the b-values, which range from 0.6 to 1.3 over the fault plane. The comparison between the spatial distribution of the b-values and the main-shock slip pattern shows that the largest slip occurs in normal-to-high b-values portion of the fault plane, while low b-value is observed close to the main-shock nucleation. No substantial differences are found in the b-value computed before and after the main-shock struck in the region of the fault plane populated by foreshocks.

Introduction

Rupture complexity during large earthquakes is usually explained in terms of stress or strength heterogeneity along the fault plane: asperity [Kanamori and Stuart, 1978; Ruff, 1992] and barrier [Das and Aki, 1977]. These two different models explain also the occurrence of foreshocks, small asperities that rupture before the main event, and aftershocks, small barriers unbroken during the main event. The occurrence of both foreshocks and aftershocks during seismic sequences indicates that a mixture of stress and strength heterogeneities co-exists in the rupture process.

The frequency-magnitude relationship has been used to map asperities along major faults, with the idea that the b-value is sensitive to highly stressed, locked portions of the crust [Wiemer and Wyss, 1997; Schorlemmer and Wiemer, 2005; Ghosh et al., 2008]. The lower the b-value the higher the applied shear stress [Wyss et al., 2000; Wyss et al., 2004]. In accordance, low b-value is observed close to the nucleation zone of large earthquakes [Nuannin et al., 2005; Schorlemmer and Wyemer, 2005] and proposed as a good proxy for sizing the asperities capable of large slip. The analysis of aftershocks revealed that high b-value regions are correlated with the highest slip during large earthquakes [Görgün et al., 2009; Sobiesiak et al., 2007]. Although the variation of the b-value along a fault is often observed and resolved, a physical interpretation of what locally alters the frequency-magnitude relationship, changes in the state of stress and/or material properties is still lacking [Wiemer and Katsumata, 1999]. Mori and Abercombie [1997] interpreted the decrease of the b-value with increasing depth, observed for earthquakes in California, as due to a diminution of the heterogeneity with depth. Laboratory experiments [Amitrano, 2003] suggest that b-values reflect the type of macroscopic behavior (brittle-ductile) and the b-decrease with depth can be due to change from brittleness to ductility.

In this study, we present the b-value distribution along the 2009 L'Aquila fault, probably the best-monitored normal faulting earthquake occurred so far [Chiarabba et al., 2009]. The analysis of the closest strong motion accelerograms reveals that the initial stages of the main shock rupture are rather complex. Indeed, ground motion time histories show an initial emergent P-wave signal (hereinafter EP) followed by an impulsive onset (IP) (see Figure 1 and 3) [Di Stefano et al., 2011]. An almost null slip is observed close to the hypocenter, while the largest slip patch (up to 1 meter, see Figure 3) is located southeastward of the rupture nucleation [Atzori et al., 2009; Cirella et al., 2009; Trasatti et al., 2011], in agreement with the evidence of rupture directivity toward SE [Pino and Di Luccio, 2009]. The delayed along-strike propagation has been explained in terms of heterogeneity of material properties [Cirella et al., 2009; Di Stefano et al., 2011]. Main objective of this study is to verify if the distribution of b-value along the fault plane contributes to improve our understanding of the physical process at the base of moderate to large earthquakes.

Data and Method

We consider all the aftershocks occurred until the end of 2009 and relocate them using the 1-D (P- and S-wave) velocity model of Chiaraluce et al. [2011]. We retain only events with at least 4 P- and 1 S-phases, hypocenter solution with rms < 0.5 s, azimuthal gap < 180°, and formal errors < 1 km. Finally, we select all the earthquakes located within 5 km of perpendicular distance from the fault plane, as identified by Di Stefano et al. [2011], (Figure 1). This gives us a set of 7,634 events.

We first assess the level of completeness of the used catalog, an issue that is especially critical in the first few days after a main-shock, due to under-reporting of short-term aftershocks [Enescu et al., 2007]. Also, in our case, changes in the magnitude of completeness (M_C) arise from the increased monitoring capabilities after a number of temporary seismic stations starts to operate in the meizoseismal area [Margheriti et al., 2011]. We compute the M_C vs time relationship for the selected aftershock catalog on running windows of 300 events (Figure 2a). On each sample, we determine the magnitude of completeness (M_C) as the magnitude at which 90% of the data can be modeled by a power law fit [Wiemer and Wyss, 2000]. Uncertainties on the M_C values were calculated by bootstrapping each sample with 1000 realizations, and indicated with dashed lines in Figure 2a. We consider that the M_C reaches a stable value when a straight line fitting data points becomes horizontal (slope = 0.0), within their uncertainties (Figure 2b). This condition is verified starting from the end of day 5 after the main-shock (see Figure 2b), when M_C is about 1.5. We therefore split the aftershocks into two sub-catalogs, the first one (C_1) from the main-shock to day 5 (04/10/2009), the second one (C_2) from day 6 (04/11/2009) to the end of 2009.

We compute the distribution of b-value—as well as complementary seismicity parameters—on the fault plane relative to C_2, i.e. after the M_C reaches a steady threshold, which contains 5,527 earthquakes. Uniform detection sensitivity over the whole fault plane is assumed. All the selected earthquakes are projected on the fault plane. Calculations are made by dividing the fault plane into 5x5 km square cells. In each cell containing at least 100 earthquakes M_C, b-value, a-value, and number of events above M_C (N_{MC}) are computed (this last only shown in the auxiliary material), following the *maximum likelihood estimate* approach [Aki, 1965] described by Wiemer and Wyss [2000]. Cells are retained only if the error on the b-value does not exceed 10% of its estimate [Shi and Bolt, 1982]. The grid is then shifted along the directions of the cell edges by half of cell size and calculations are re-made, thus obtaining a 2.5x2.5 grid. A continuous representation of the estimated parameters on the fault plane (Figure 3a-d) is obtained through a common minimum curvature gridding method [Smith and Wessel, 1990]. The corresponding discrete representation is available on the auxiliary material (Figure S1).

We then compare the distribution of b-value on the fault plane relative to C_2 to those obtained for C_1 (2,107 earthquakes). For C_1 calculations are made following two different approaches: fixing the M_C over the whole fault plane to its worst value (M_C = 2.5, see Figure 2a); estimating in each cell its own M_C, as for the C_2. The results of this exercise are shown in Figure 3e,f (for a full discrete representation of the parameters obtained for C_1, see Figure S2 and Figure S3 in the auxiliary material).

Finally, we compare the distribution of the b-value obtained from the aftershocks analysis (Figure 3c,e,f) with the b-value computed for the foreshock sequence preceding the M_W 6.1 L'Aquila earthquake (Figure 3d) [see Lucente et al., 2010, for the foreshock sequence details]. The seismicity parameters on the fault plane region populated by the foreshocks are computed by estimating in each cell its own M_C, as for the C_2 (for a full discrete representation of the seismicity parameters computed for the foreshock sequence, see Figure S4 in the auxiliary material).

Results

In the following we summarize the main results of our analysis. For the sake of simplicity, we will refer to C_1 and C_2 aftershock catalogs as C_1 and C_2 periods of the aftershock sequence. We base the general description of the seismicity parameters on the values obtained for the C_2 period, i.e. when the M_C reaches a stable value. The b-value distribution obtained for the C_1 period and for the foreshocks sequence is also discussed and the significance of the b-value variation through the different periods is assessed.

The frequency-magnitude relationship of the aftershocks features a low b-value in the nucleation zone and a normal-to-high b value (0.9-1.1) on the fault portion with the highest coseismic slip (Figure 3c). b-values higher than 1.1 are observed in the upward tip of the fault, upside the large slip area (Figure 3c).

Low b-values, below 0.8, are observed in the northwestern deep portion of the fault plane, also prior to the major seismic event (Figure 3d) and in C_1 period (Figure 3f), when in each cell its own M_C is estimated. Also for fixed M_C in C_1, this portion of the fault plane features the lowest b-values (lower than 1.0, cfr. Figure 3e). This low b-value region, close to the nucleation zone, coincides with the area interested by most of the early strong aftershocks (Figure 3e,f). The non-overlapping of low b-value and highest M_C regions both in period C_1 and C_2 (see Figure S1a,c and Figure S3a,c in the auxiliary material) enables us to exclude a b-value underestimation due to inclusion of earthquakes below M_C. Again, high values of b (above 1.0) characterize the higher slip area in the C_1 period (Figure 3e,f).

We point out that, although the b-values computed for the C_1 period differ by 0.2 on average (Figure 3e,f), depending on the computation approach used, the distribution of areas of relative maximum and minimum b-values on the fault plane remains unchanged, providing equivalent information. We assess the significance of these differences by applying the statistical test proposed by Amorèse et al. [2010] (see auxiliary material): the differences observed in the b-values computed for the C_1 period using the two different approaches are not significant from a statistical point of view.

We evaluate the significance of the temporal variation of b-value from the foreshock through the C_1 and C_2 periods by applying the same statistical test [Amorèse et al., 2010] (see auxiliary material). We only find a significant temporal variation of b-value between period C_2 and C_1 (both approaches) in the northwestern deep portion of the fault plane (see Figure 3e,f of the main text and Figure S2 and S3 in the auxiliary material). Here the b-value increases from about 0.6 to about 1.0 after the first five days. In all the other cells the variation of b-value is not significant by a statistical point of view. No significant differences are found between the b-values computed for the foreshock catalog and the b-values computed for each of the aftershock sub-catalogs, C_1 (both approaches) and C_2.

Discussion and Conclusions

By using the b-value as a stress-meter, as suggested by Schorlemmer and Wiemer [2005], we infer that the nucleation region is at the edge of the highly stressed portion of the fault, since the low b-values observed by the foreshocks and the early part of the aftershock sequence (C_1 period). This is in accordance to the results of laboratory fracture studies on rock samples, where low b-values correspond to the asperity regions and initiation of the main events rupture at the edge of asperities is by far the most common instance [Lei, 2003; Goebel et al., 2012]. The foreshock activity all occurred within the low b-value zone (see Figure 3d). During the rupture, the low b small fault patch experienced a null or low slip (Figure 3c). Then the stress variation by the main-shock caused the rupture of intact neighboring asperities and large aftershocks occurred (see Figure 3e,f). In the large slipping portion of the fault, the shear stress drops significantly during the main rupture and favors high b-value for the aftershocks (Figure 3c,e,f) [Wiemer and Katsumata, 1999]. The normal-to-high b-value defined by aftershocks that occurred in the high slip area is consistent with observations for other large earthquakes [Wiemer and Katsumata, 1999; Wiemer et al., 2002; Zhao and Wu, 2008]. In this area, shear stress are almost entirely released by the main-shock and few strong aftershocks occur (Figure 3c,e,f). The statistically significant increase of b-value for C_2 (see Figure 3c) in the low b-value zone seen in the C_1 period, could indicates a coseismic stress-drop and a consequent redistribution of the stress, as observed for both natural sequences and laboratory experiments [Schorlemmer and Wiemer, 2005; Lei, 2003].

The low b-values area close to the nucleation, strictly coincides with a high V_P, low Poisson ratio volume, while the high b-values in the upper portion of the fault are corresponds to high Poisson ratio [Di Stefano et al., 2011]. This last observation is consistent with diffuse aftershocks spreading over a large shallow volume favored by a progressive upward migration of fluids. In this shallow region afterslip occurred, as modeled by geodetic data [Cheloni et al., 2010; Lanari et al., 2010]. It’s worth to note that, the area of resolved increased b-value, in the northwestern deep portion of the fault plane, corresponds at least partially to the deepest patch of postseimic afterslip modeled from the inversion of multitemporal DInSAR and GPS measurements made since 6 days from the main-shock [D’Agostino et al., 2012].

We conclude that, if the low b-value is really sizing the asperities, then the set of observations arising from the distribution of the b-value along the fault responsible for the L'Aquila earthquake support the idea that location of the asperities on the fault plane plays a crucial role in determining the spatial properties of both nucleation and slip areas. Furthermore, it seems to be a major factor in controlling location and size of both fore- and after-shock events.

References

Aki, K. (1965), Maximum likelihood estimate of b in the formula log N = a – bM and its confidence limits, *Bull. Earthquake Res. Inst. Univ. Tokyo, 43*, 237–239.

Amitrano, D. (2003), Brittle-ductile transition and associated seismicity: Experimental and numerical studies and relationship with the b-value, *J. Geophys. Res., 108*, doi:10.1029/2001JB000680.

Amorèse, D., J. R. Grasso, and P. A. Rydelek (2010), On varying b-values with depth: Results from computer-intensive tests for Southern California, *Geophys. J. Int., 180*, 347–360, doi 10.1111/j.1365-246X.2009.04414.x.

Atzori, S., I. Hunstad, M. Chini, S. Salvi, C. Tolomei, C. Bignami, S. Stramondo, E. Trasatti, A. Antonioli, and E. Boschi (2009), Finite fault inversion of DInSAR coseismic displacement of the 2009 L'Aquila earthquake (central Italy), *Geophys. Res. Lett., 36*, L15305, doi:10.1029/ 2009GL039293.

Cheloni, D., et al. (2010), Coseismic and initial post-seismic slip of the 2009 Mw 6.3 L'Aquila earthquake, Italy, from GPS measurements, *Geophys. J. Int., 181*, 1539–1546, doi:10.1111/j.1365-246X.2010.04584.x.

Chiarabba, C., et al. (2009), The 2009 L'Aquila (central Italy) Mw 6.3 earthquake: Main shock and aftershocks, *Geophys. Res. Lett., 36*, L18308, doi:10.1029/2009GL039627.

Chiaraluce, L., L. Valoroso, D. Piccinini, R. Di Stefano, and P. De Gori (2011), The anatomy of the 2009 L'Aquila normal fault system (central Italy) imaged by high resolution foreshock and aftershock locations, *J. Geophys. Res., 116*, B12311, doi:10.1029/2011JB008352.

Cirella, A., A. Piatanesi, M. Cocco, E. Tinti, L. Scognamiglio, A. Michelini, A. Lomax, and E. Boschi (2009), Rupture history of the 2009 L'Aquila (Italy) earthquake from non linear joint inversion of strong motion and GPS data, *Geophys. Res. Lett., 36*, L19304, doi:10.1029/2009GL039795.

D'Agostino, N., D. Cheloni, G. Fornaro, R. Giuliani, and D. Reale (2012), Space-time distribution of afterslip following the 2009 L'Aquila earthquake, *J. Geophys. Res.*, *117*, B02402, doi:10.1029/2011JB008523.

Das, S., and K. Aki (1977), Fault plane with barriers-versatile earthquake model, *J. Geophys. Res.*, *82*, 5658–5670, doi:10.1029/JB082i036p05658.

Di Stefano, R., C. Chiarabba, L. Chiaraluce, M. Cocco, P. De Gori, D. Piccinini, and L. Valoroso (2011), Fault zone properties affecting the rupture evolution of the 2009 (Mw 6.1) L'Aquila earthquake (central Italy): Insights from seismic tomography, *Geophys. Res. Lett., 38*, L10310, doi:10.1029/2011GL047365.

Enescu, B., J. Mori, and M. Miyazawa (2007), Quantifying early aftershock activity of the 2004 mid-Niigata Prefecture earthquake (Mw6.6), *J. Geophys. Res., 112*, B04310, doi:10.1029/2006JB004629.

Görgün, E., A. Zang, M. Bohnhoff, C. Milkereit, and G. Dresen (2009), Analysis of Izmit aftershocks 25 days before the November 12th 1999 Düzce earthquake, Turkey, *Tectonophysics, 474*, doi:10.1016/j.tecto.2009.04.027.

Ghosh, A., A. V. Newman, A. M. Thomas, and G. T. Farmer (2008), Interface locking along the subduction megathrust from b-value mapping near Nicoya Peninsula, Costa Rica, *Geophys. Res. Lett., 35*, L01301, doi:10.1029/2007GL031617.

Goebel, T. H. W., T. W. Becker, D. Schorlemmer, S. Stanchits, C. Sammis, E. Rybacki, and G. Dresen (2012), Identifying fault heterogeneity through mapping spatial anomalies in acoustic emission statistics, *J. Geophys. Res., 117*, B03310, doi:10.1029/2011JB008763.

Kanamori, H., and G. S. Stewart (1978), Seismological aspects of the Guatemala earthquake of February 4, 1976, *J. Geophys. Res., 83*, 3427–3434, doi:10.1029/JB083iB07p03427.

Lanari, R., et al. (2010), Surface displacements associated with the L'Aquila 2009 Mw 6.3 earthquake (central Italy): New evidence from SBAS-DInSAR time series analysis, *Geophys. Res. Lett., 37*, L20309, doi:10.1029/2010GL044780.

Lei, X. (2003), How do asperities fracture? An experimental study of unbroken asperities,
Earth Planetary Sci. Letts., 26, 247–258.

Lucente, F. P., P. De Gori, L. Margheriti, D. Piccinini, M. Di Bona, C. Chiarabba, and N. Piana Agostinetti (2010), Temporal variation of seismic velocity and anisotropy before the 2009 MW 6.3 L'Aquila earthquake, Italy, *Geology, 38(11)*, 1015–1018, doi:10.1130/G31463.1.

Margheriti, L., et al. (2011), Rapid response seismic networks in Europe: lessons learnt from the L'Aquila earthquake emergency, *Annals of Geophysics*, *54*; doi: 10.4401/ag-4953.

Mori, J., and R. E. Abercrombie (1997), Depth dependence of earthquake frequency-magnitude distributions in California: Implications for rupture initiation, *J. Geophys. Res.*, *102*, 15,081–15,090.

Nuannin, P., O. Kulhanek, and L. Persson (2005), Spatial and temporal b-value anomalies preceding the devastating off coast of NW Sumatra earthquake of December 26, 2004, *Geophys. Res. Lett., 32*, L11307, doi:10.1029/2005GL022679.

Pino, N. A., and F. Di Luccio (2009), Source complexity of the 6 April 2009 L'Aquila (central Italy) earthquake and its strongest aftershock revealed by elementary seismological analysis, *Geophys. Res. Lett.*, *36*, L23305, doi:10.1029/2009GL041331.

Ruff, L.J. (1992), Asperity distributions and large earthquake occurrence in subduction zones, *Tectonophysics, 211(1-4)*, 61–83.

Schorlemmer, D., and S. Wiemer (2005), Microseismicity data forecast rupture area, *Nature*, *434*, 1086, doi:10.1038/4341086a.

Shi, Y., and B. A. Bolt (1982), The standard error of the magnitude-frequency b-value, *Bull. Seism. Soc. Am., 72*, 1677–1687.

Smith, W.H.F., and P. Wessel (1990), Gridding with continuous curvature splines in tension, *Geophysics, 55*, 293–305.

Sobiesiak, M., U. Meyer, S. Schmidt, H.-J. Gotze, and C. M. Krawczyk (2007), Asperity generating upper crustal sources revealed by b-value and isostatic residual anomaly grids in the area of Antofagasta, Chile, *J. Geophys. Res., 112*, doi:10.1029/2006JB004796.

Trasatti, E., C. Kyriakopoulos, and M. Chini (2011), Finite element inversion of DInSAR data from the Mw 6.3 L'Aquila earthquake, 2009 (Italy), *Geophys. Res. Lett., 38*, L08306, doi:10.1029/2011GL046714.

Wiemer, S., M. Gerstenberger, and E. Hauksson (2002), Properties of the aftershock sequence of the 1999 Mw 7.1 Hector Mine earthquake: implications for aftershock hazard, *Bull. Seism. Soc. Am., 92(4)*, 1227–1240.

Wiemer, S., and K. Katsumata (1999), Spatial variability of seismicity parameters in aftershock zones, *J. Geophys. Res*, *104*, 13135–13151.

Wiemer, S., and M. Wyss (1997), Mapping the frequency–magnitude distribution in asperities: an improved technique to calculate recurrence times?, *J. Geophys. Res.*, *102*, 15115–15128.

Wiemer, S., and M. Wyss (2000), Minimum magnitude of complete reporting in earthquake catalogs: Examples from Alaska, the western United States, and Japan, *Bull. Seismol. Soc. Am., 90,* 859–869.

Wyss, M., C. G. Sammis, R. M. Nadeau, and S. Wiemer (2004), Fractal dimension and b-value on creeping and locked patches of the San Andreas fault near Parkfield, California, *Bull. Seismol. Soc. Am., 94(2),* 410–421.

Wyss, M., D. Schorlemmer, and S. Wiemer (2000), Mapping asperities by minima of local recurrence time: The San Jacinto-Elsinore fault zones, *J. Geophys. Res., 105,* 7829–7844.

Zhao, Y. Z., and Z. L. Wu (2008), Mapping the b-values along the Longmenshan fault zone before and after the 12 May 2008, Wenchuan, China, Ms 8.0 earthquake, *Nat. Haz. Earth Syst. Sci., 8,* 1375–1386.

Figure Captions

Figure 1. Map of the L'Aquila earthquake aftershocks used in this study. Earthquakes are color-coded by depth according to the scale on top. The yellow stars indicate the locations of the EP and IP phases of the main-shock, respectively (see text for details). The red dashed box on map outlines the surface projection of the main shock fault plane [Di Stefano et al., 2011], where thicker red hatched line indicates its top edge. Triangles are seismic stations operating in the meizoseismal area during the aftershock sequence: permanent (red triangles) and installed after the main-shock (pink triangles). In the bottom right inset a cross section through the main-shock is drawn (see thin black line on map). Again the yellow stars represent the EP (smaller) and IP (larger) phases of the main-shock, while the red line is the trace of the fault plane. We project on the cross section all the events located within 2 km distance from the vertical plane and 5 km from the fault plane (see text for details). Star in the bottom left inset is location of the L'Aquila main shock on map of Italy.

Figure 2. (a) M_C as a function of time for the aftershock catalog used in this study (detail of the first 30 days from the main-shock). Thick line represent the M_C values computed on running windows of 300 events, dashed lines indicate its standard deviation. Frequency of data points can be seen on the plot below. (b) Slope of the straight line fitting the M_C *vs time* data points in the above plot. Each point represents, on the time scale, the slope of the straight line fitting all points from that moment onward, until the end of 2009. On each point, vertical bars indicate the standard deviation of the slope.

Figure 3. Continuous representation of seismicity parameters on the L'Aquila earthquake fault plane shown in Figure 1. The first three panels display: (a) M_C, (b) a-value, and (c) b-value obtained for C_2 sub-catalog, respectively (see text for details). Last three panels display the b-values computed for (d) the foreshock catalog and for the C_1 sub-catalog in the case of (e) fixed and (f) changing M_C, respectively (see text for details). Below each panel the appropriate color scale is placed. On each panel black stars indicate the locations on the fault plane of the EP (smaller) and IP (larger) phases of the main-shock. On panel (a) the orientation of the fault plane is indicated. On panels representing the b-value (c-f), earthquakes used for the analysis in their respective cases are also shown ($M_L < 3.5$ = small black dots; $M_L > 3.5$ = red circles), along with the co-seismic slip by Cirella et al. [2009] (black solid contouring). Finally, on panels representing the b-value computed for the C_1 sub-catalog, (e) and (f) (both approaches, see text for details), the shaded area on the bottom-left outlines the cells in which the difference of b-value with respect to that computed for C_2 is statistically significant [Amorèse et al. 2010].

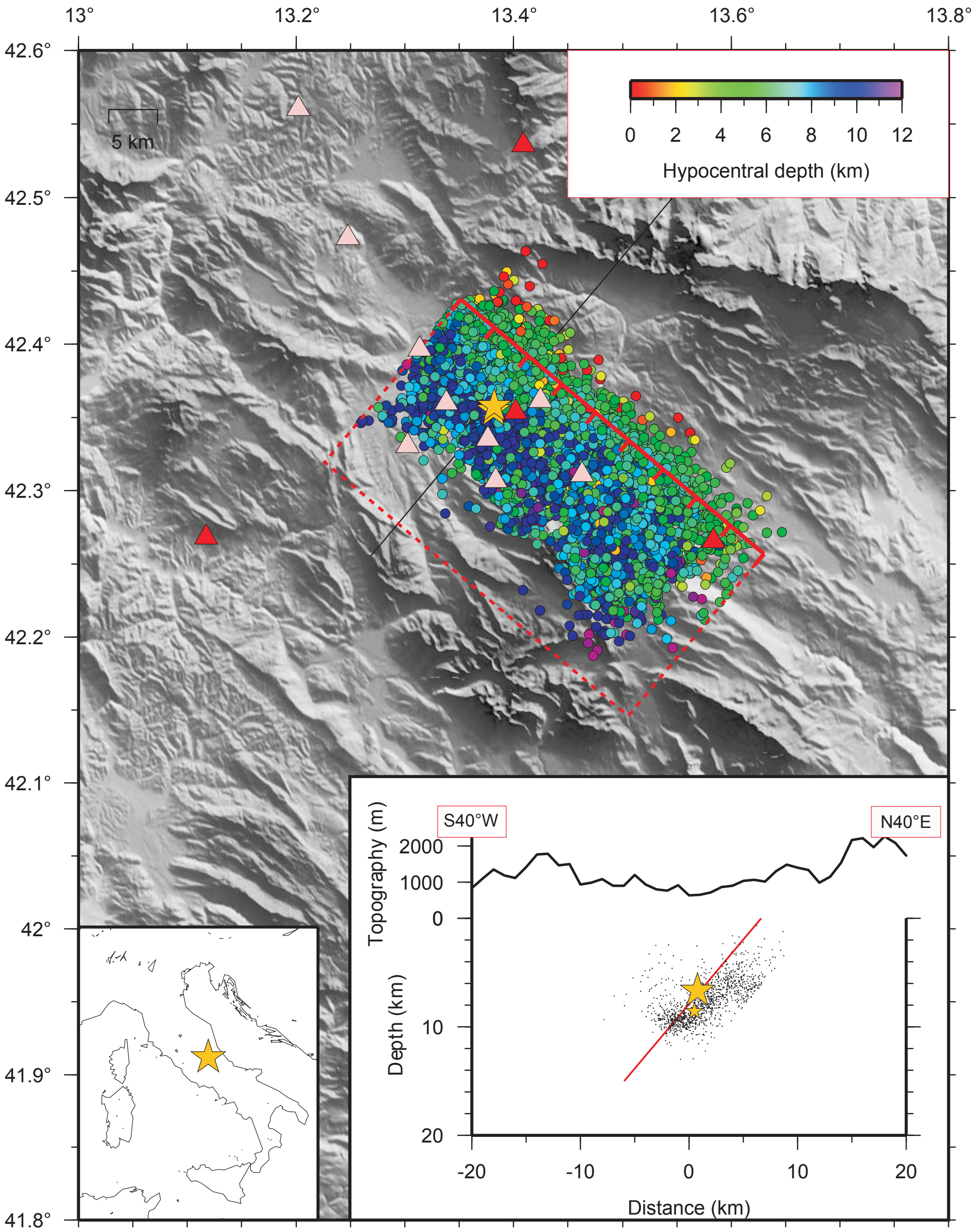

13°
13.2°
13.4°
13.6°
13.8°
42.6°
42.5°
42.4°
42.3°
42.2°
42.1°
42°
41.9°
41.8°
5 km
0 2 4 6 8 10 12
Hypocentral depth (km)
S40°W
N40°E
Topography (m)
2000
1000
0
Depth (km)
10
20
-20 -10 0 10 20
Distance (km)

Figure 1

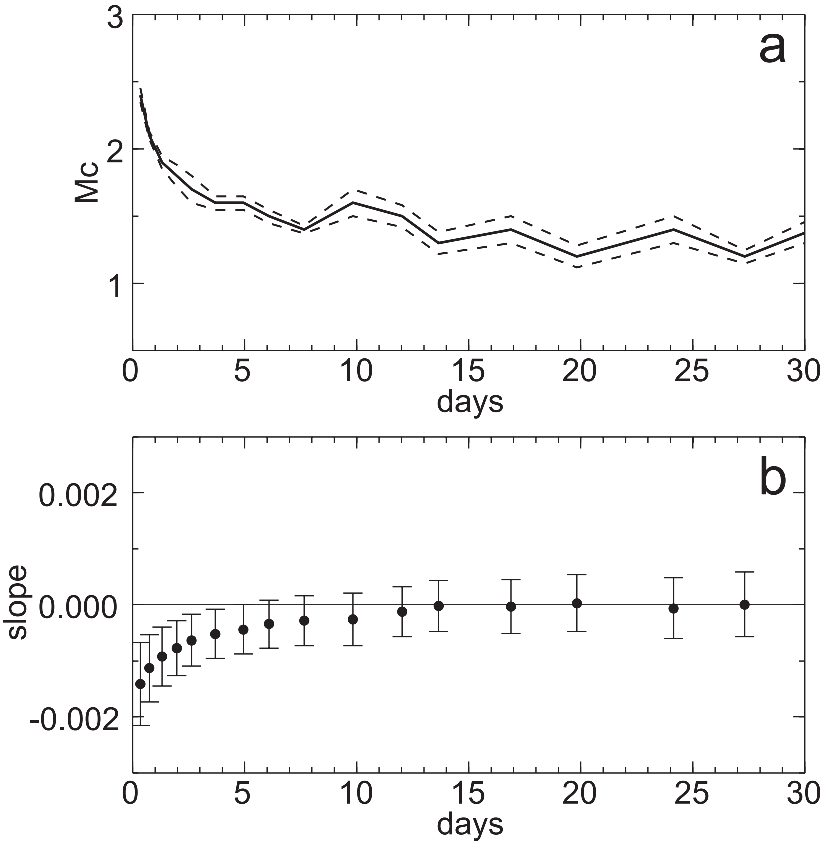
3
a
2
Mc
1
0
5
10
15
20
25
30
days
b
0.002
slope
0.000
-0.002
0
5
10
15
20
25
30
days

Figure 2

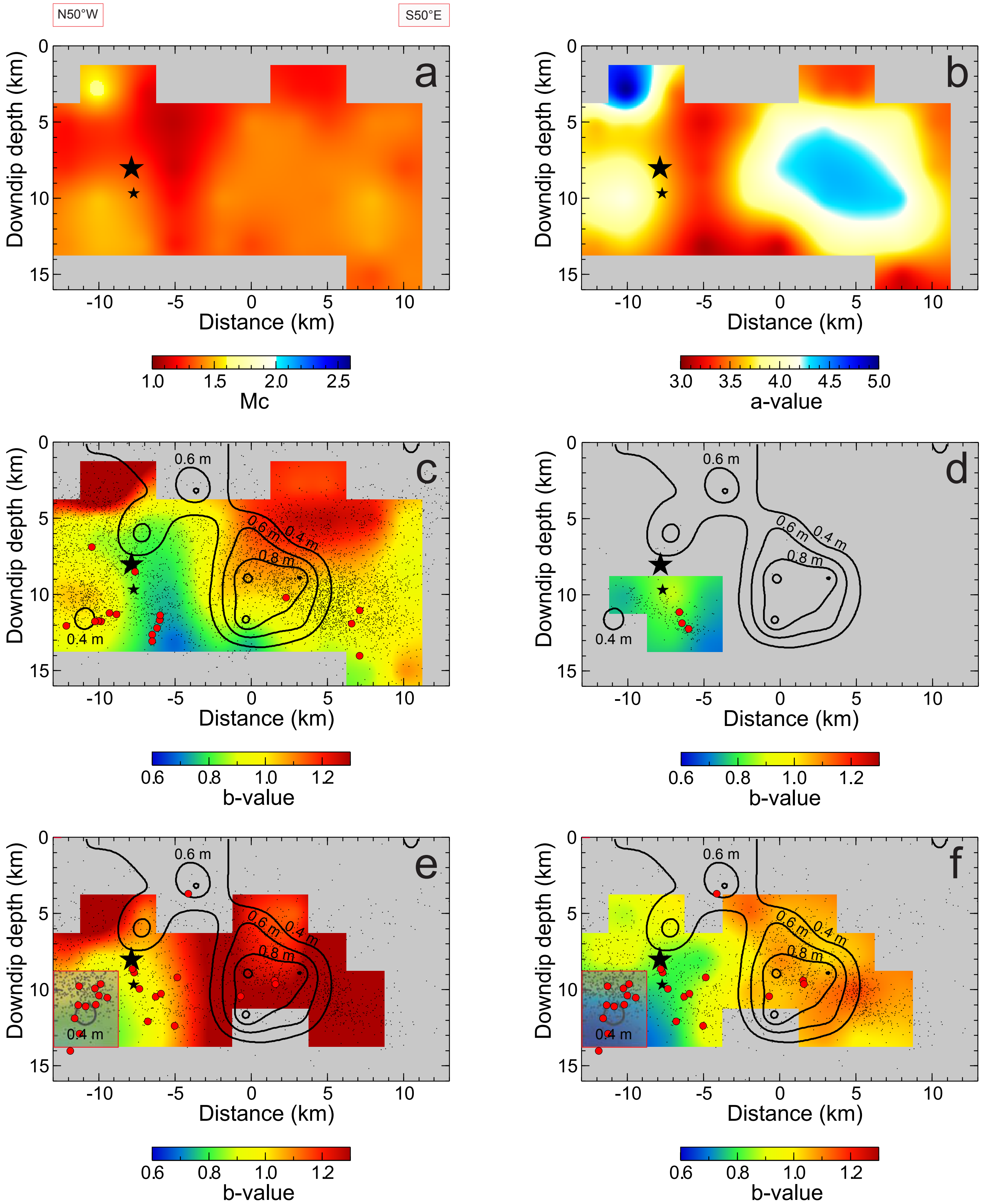

N50°W
S50°E
a
b
c
d
e
f
Downdip depth (km)
Distance (km)
Mc
a-value
b-value
0.6 m
0.4 m
0.8 m

Figure 3